UDC 004.89

Classification of Structural and Functional Development Stage of Cardiomyocytes Using Machine Learning Techniques

Bondarev V. R., Ivanko K. O., Ivanushkina N. G.

Electronic Engineering Department, Faculty of Electronics,
National Technical University of Ukraine "Igor Sikorsky Kyiv Polytechnic Institute", Kyiv, Ukraine

E-mail: *vbondarev-ee23@lll.kpi.ua, ivanko-ee@lll.kpi.ua, niva-ee@lll.kpi.ua*

The study is dedicated to the problem of classification of structural and functional development stage of cardiomyocytes derived from the induced pluripotent stem cells with application of the digital image processing methods and machine learning algorithms, in particular, neural networks. Cell regenerative therapy has become one of the most promising treatment options for patients with heart failure. But since cardiomyocytes are objects with a high level of complexity and have significant morphological variability, automatic classification is complicated by the lack of implemented methods. That's why researches in this area are a major global public health priority. The initial data set used in this study is a publicly open set of confocal microscopic images of cardiomyocytes which can be divided into five classes based on the morphological features (the structure of the transverse T-tubule). A small amount of input data leads to the need of using augmentation methods. Methods that prevent the alteration of the transverse T-tubule, which is an important parameter for correct classification of the development of cardiomyocytes, are used. Histogram equalization technique is used to enhance the contrast and dynamic range of the confocal microscopic images with the method of contrast-limited adaptive equalization. This helped to improve the local contrast of the analyzed images and highlight the main elements of the cardiomyocyte. Finally, Chan–Vese method, which belongs to the regional segmentation methods, is chosen for the image segmentation and removing artifacts and/or parts of other cells from the image. A pre-processed and augmented dataset is used for training of the convolutional neural network having an architecture with hierarchical structure and residual block usage. The model is evaluated based on the confusion matrix and the heat maps of different convolutional layers are analyzed. Images from the classes with a large number of mutual errors are also considered. Based on the analysis, several classes of structural and functional development of cardiomyocytes are combined. Final accuracy of the model for defining the cardiomyocytes maturation stage achieved 77%.

Keywords: cardiomyocyte; stem cells; image processing; machine learning; machine learning problem; classification; classification accuracy; neural network; convolutional neural network

Introduction

Heart failure is a pathological condition that occurs as a result of various heart diseases that reduce the pumping capacity of the heart, resulting in insufficient blood circulation in the human body [1]. The main cause of acute heart failure is acute coronary syndrome [1].

Acute heart failure is a common pathological condition and one of the most common causes of total mortality (16% of the world's total deaths [2]). According to estimates, 1.5-2% of the entire population have signs of chronic heart failure [2]. The frequency of chronic heart failure increases with age, and according to estimates, it occurs in 3-5% of people over 65 years of age, and for people over 75 years of age, the frequency of heart failure is 10% [2]. Heart failure affects more than 64 million people worldwide. Therefore, attempts to decrease its social and economic burden have become a major global public health priority [3].

Cell regenerative therapy has become one of the most promising treatment options for patients with heart failure. Cardiomyocytes (contractile myocytes of the heart muscle, which ensure the work of the heart [4]) from human embryonic stem cells (ESCs) and human induced pluripotent stem cells (PSCs) show great opportunity as potential cell sources for cardiac repair [5]. Both of these pluripotent stem cell types have clear cardiomyogenic potential, which favorably distinguishes them from many types of adult stem cells, for which the ability to differentiate into a significant number of definitive cardiomyocytes is controversial [5]. In addition, both undifferentiated ESCs and PSCs exhibit potent proliferative activity,

making these cell types particularly attractive for cases that require large numbers of cells (eg, replacement of $\sim 1 \times 10^9$ cardiomyocytes lost after a typical myocardial infarction) [6]. Cardiomyocytes derived from ESCs and PSCs have an unambiguous cardiac phenotype, showing spontaneous contractile activity and cardiac mechanisms of excitation-contraction coupling [6].

Studies conducted on animal models show that cardiomyocytes grown from PSC can partially remuscularize heart infarction and improve contractile function [7]. Caspi and colleagues demonstrated by echocardiography the survival of PSC-CM grafts in infarcted rat hearts at 8 weeks post-transplantation, and improvements in the left ventricular size and function in cardiomyocyte recipients compared with controls at 4 and 8 weeks post-transplantation [8]. Moreover, Shimizu and colleagues developed an approach based on the scaffold-free cell sheets transplanted directly onto the surface of the heart. Cells can be efficiently delivered in the form of thin but dense large-area cell constructs without cell loss [9]. In general, positive trends in the research in this area and increasing of the transplantation efficiency should be noted.

There are several approaches to evaluating cardiomyocytes grown from the pluripotent stem cells. One of them is the measurement of the contractile ability of cells [10]. Along with it, measurements of transient Ca2+ processes are performed [10]. These functional tests allow to assess the quality of the grown cardiomyocytes population. The process of growing cardiomyocytes from the pluripotent stem cells can be divided into several stages [11] and the indicated tests depend on the development stage. Given the above, the development stage is evaluated by morphological features using confocal microscope images [10].

Currently, there are several significant limitations in the cultivation of cardiomyocytes and studies of their development stages. For statistical analysis of the entire population, it is necessary to assign a developmental stage to each observed cardiomyocyte image according to a complex set of object features and classification rules [10]. This approach is impractical and prone to subjective errors. Considering the amount of data required for statistical analysis, automatic image classification is more appropriate. Since cardiomyocytes are objects with a high level of complexity and have significant morphological variability, automatic classification is complicated by the lack of implemented methods.

Therefore, this study considers and applies the main methods of digital image processing and machine learning algorithms including neural networks for the task of determining the stage of structural and functional maturation of cardiomyocytes.

1   Materials and Methods

The data set used in this study is the publicly available database Confocal Microscopy Images of Cardiomyocyte Development Stages from IEEE DataPort platform [12]. Regarding the specification [12], cardiomyocytes are divided into five classes of the development stage based on the morphological features. The first stage of maturation is characterized by the lack of the membrane inclusions. The presence of short ($\sim 2\mu$m), evenly spaced perpendicular inclusions of the membrane and/or individual long ($>10\ \mu$m) tubules can be attributed to the second stage. In the third stage, there is a network of longer tubules ($>10\ \mu$m) with both transverse and longitudinal inclusions. The fourth stage of maturation is classified by a complex system of transverse tubules with the obvious presence of longer ($>2\ \mu$m) longitudinal tubules and frequent areas devoid of tubules. The fifth stage of maturation is typical for adult cardiomyocytes and can be characterized by a complex system of transverse tubules, with sparse longitudinal structures that usually cover no more than 1-2 sarcomeres (from $\sim 2\mu$m to $\sim 4\mu$m), filling the entire area of the cell, except for the nuclei (Fig. 1).
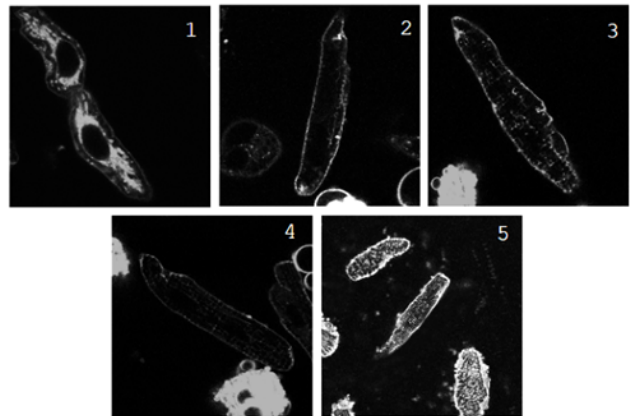

Fig. 1. Confocal images of cardiomyocytes according to their developmental stage

There are several limitations to obtaining images by confocal microscopy. Only a part of such collected images are high-quality images of intact and healthy myocytes. The rest of the dataset consists of blank images, images of dead cardiomyocytes, defocused images of cardiomyocytes, and images of cell fragments. Thus, after excluding poor-quality confocal images, a total number of high-quality images available from the dataset [12] is 111: 18 images for the first stage of cardiomyocyte maturation, 23 for the second stage, 22 for the third stage, 22 for the fourth, and 26 for the fifth stage. All images have a dimension of [1024; 1024] pixels in the grayscale spectrum [12].

For further application of machine learning methods, it is necessary to create a class-balanced data set. There are two approaches to solving the problem. The first one is to choose the number of images in each

class according to the minimum amount (in this case 18 images) with the use of the unused data to evaluate the trained model. The second approach is the use of augmentation to equalize the number of images in each class, which is chosen.

Confocal microscopy images of cardiomyocytes contain artifacts and/or parts of other cells. Segmentation methods should be used to obtain images of healthy and whole cells prior to further processing. Moreover, analyzed images in grayscale format require additional processing of their brightness histogram to improve image contrast, which positively affects the quality of further machine learning. Also, a small number of input images does not allow effective training. Thus, the training data set must be pre-processed using segmentation of the input images, processing of the brightness histogram of the segmented images and augmentation (obtaining new images from the pre-processed images).

The Chan-Vese method, which belongs to the methods of region-based segmentation, is chosen as a segmentation method [13,14]. Region-based models use the statistical information of the image such as amplitude, jumps in amplitude, autocorrelation function, etc. to construct boundaries, which gives many advantages. Firstly, they do not depend on the image gradient and can segment objects with weak boundaries with sufficient accuracy [13]. Secondly, by using global region information, region-based models are generally noise persistent [13]. The Chan-Vese model can be described as [13,14]

$$argmin_{c_1,c_2,C}\left(\mu \cdot Lenght(C) + v \cdot Area(inside(C)) + \right.$$
$$+\lambda_1 \int_{inside(C)} (f(x)-c_1)^2 dx +$$
$$\left. +\lambda_1 \int_{outside(C)} (f(x)-c_2)^2 dx \right), \quad (1)$$

where the first term penalizes the length of C (the boundary of a closed set) to control the regularity. The second term penalizes the enclosed area of C to control its size. The third and fourth terms penalize discrepancy between the piecewise constant model u and the input image f. Coefficients c_1 and c_2 here are values of piecewise-smooth function respectively inside and outside of C. By finding a local minimizer of this problem, segmentation is achieved as the best two-phase piecewise constant approximation u of the image f [13,14].

For additional optimization, a polygonal zone of interest is used as the initial contour. The resulting binary image is superimposed on the original image to obtain the resulting image (Fig. 2). A binary image should be understood as preserving (value "1" of a binary image) the brightness of a pixel of the input image, or reducing it to a zero value (value "0" of a binary image).

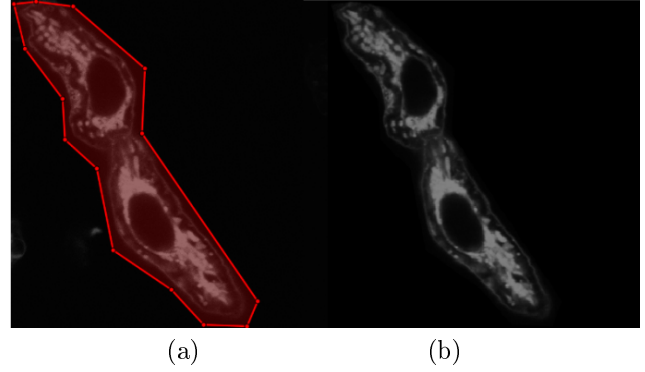(a)   (b)

Fig. 2. Input image with the polygonal zone of interest (a) and resulting image (b)

The method of contrast-limited adaptive equalization is used to process the brightness histogram, which provides the most optimal improvements of the local contrast of the image [15]. Several histograms are calculated, each of which corresponds to a separate area of the image, and are used to redistribute the brightness of the image [16].

The transformation function $f(x)$ is defined as [16]:

$$f(x) = X_0 + (X_{L-1} - X_0)\,c(x), \quad (2)$$

where X_0, X_{L-1} are L discrete gray levels and $c(x)$ is probability density function [16]:

$$c(x) = \sum_{j=0}^{k} \frac{n_k}{N}, \quad (3)$$

where n_k represents the number of times the level X_k is present in the input image x, N is the total number of components in the input image [16].

Adjacent parts of the grid are merged using interpolation methods to eliminate artificial boundaries [16]. Contrast, especially in homogeneous areas, should be limited to avoid enhancing any noise that may be present in the image (Fig. 3).

Methods that prevent alteration of the transverse T-tubule, which is an important parameter for classification, and also do not impact image contrast, are chosen as augmentation methods. To create a class-balanced data set, color inversion is chosen, which refers to color space transformations (Fig. 4) [17] and does not change the structure of cardiomyocytes [17]:

$$I_{out} = I_{max} - I_{in}\,, \quad (4)$$

where I_{max} is the maximum brightness value of a pixel in the given data type.
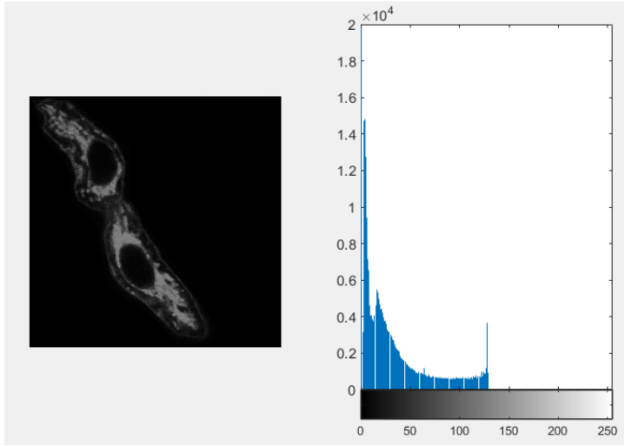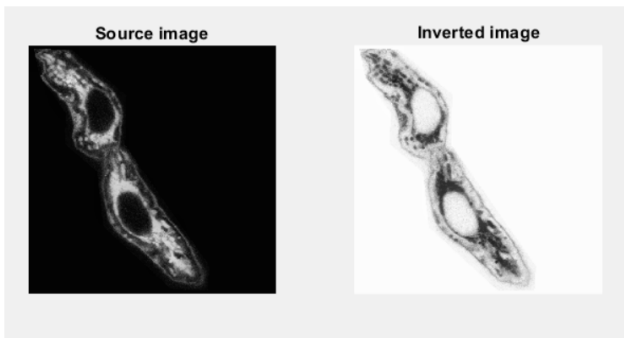
(a)
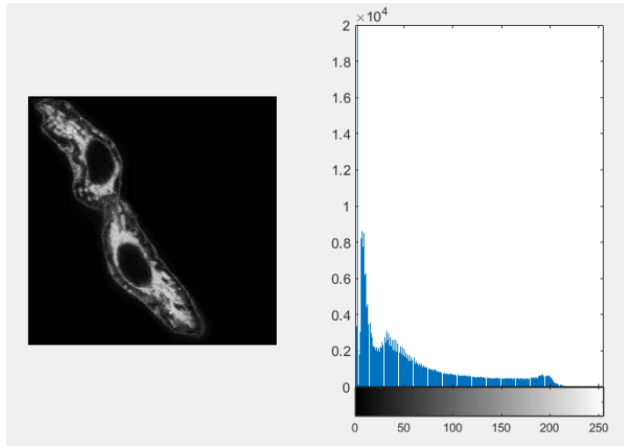
(b)

Fig. 3. Image brightness histogram processing: (a) before processing, (b) after contrast-limited adaptive equalization

(a)   (b)

Fig. 4. Color inversion of the input image: (a) before processing, (b) after color inversion

Geometric image transformations (rotation and flipping [17]) are chosen to increase the number of images (Fig. 5, Fig. 6). The new coordinates of the pixel (x_1, y_1) when rotated by an angle Θ around (x_0, y_0) are defined as [18]:

$$x_2 = \cos(\Theta) \cdot (x_1 - x_0) + \sin(\Theta) \cdot (y_1 - y_0),$$
$$y_2 = -\sin(\Theta) \cdot (x_1 - x_0) + \cos(\Theta) \cdot (y_1 - y_0). \tag{5}$$

In order to preserve the dimensionality of the image, cropping is performed.
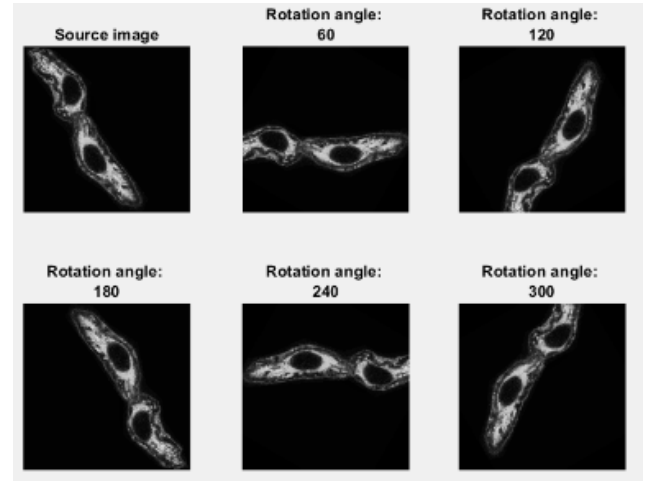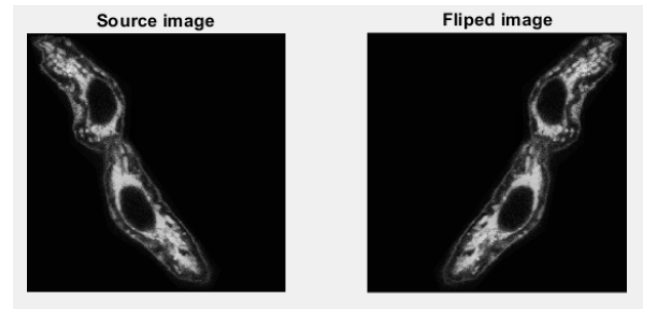

Fig. 5. Rotation of the input image

Fig. 6. Flipping of the input image

Different augmentation approaches are chosen, which allows to increase the differentiation of the data. Each image is flipped and rotated with a step of 15 degrees. This allowed us to obtain 48 new images from an original one. Color inversion is used to get a class-balanced data set with 27 original images in each class. In this way, we obtained a class-balanced data set, including 1296 images with a pre-processed brightness histogram for each class.

2   CNN model design

Convolutional neural networks (CNNs) differ from other neural networks by their high performance while working with images, speech signals, or audio signals [19].

The hierarchical structure of the CNN is used in this study. The convolutional layer applies a feature detector (two-dimensional array of weights that represents a part of the image [20]) to the image region and calculates the scalar product between the input pixels and the filter [20]. Deeper layers use features highlighted by the previous. Each individual part of the model constitutes a lower-level pattern in the neural network, and the combination of its parts represents a higher-level pattern, creating a hierarchy of features [20].

After each CNN convolution operation, a rectified linear unit (ReLU) transformation is applied to the feature map as an activation function, which also introduces nonlinearity into the model [20,21]. A rectified linear function is a piecewise linear function that outputs the input signal directly if it is positive, otherwise the output is zero:

$$f(x) = max(0, x). \qquad (6)$$

The batch normalization layer is selected as an additional layer at each layer of the hierarchical structure. This layer standardizes each batch of inputs to a certain level (performs normalization of the output vector of parameters). This makes it possible to stabilize the learning process and significantly reduce the number of learning cycles required to create a network [22].

The pooling layer (downsampling) performs dimensionality reduction by applying a weightless filter and preserving the maximum weight coefficient, reducing the number of parameters in the input data [20].

The fully connected layer solves the classification task [20] based on the features extracted by the previous layers and their filters using the average cross-entropy loss function, which can be expressed as [21]

$$Loss(\widehat{y}, y, W) =$$
$$= -\frac{1}{n} \sum_{i=0}^{n} (y_i \ln(\widehat{y_i}) + (1-y_i) \ln(1-\widehat{y_i})) + \frac{\alpha}{2n} ||W||_2^2, \qquad (7)$$

where $\widehat{y}$, y are the original and predicted values, $||W||_2^2$ penalizes complex models and $\alpha > 0$ is an integral parameter that controls the amount of the penalty [21].

In gradient descent, the loss gradient $\nabla Loss W$ with respect to the weights is calculated from W [21]:

$$W_{i+1} = W_i - \epsilon \nabla Loss_W^i, \qquad (8)$$

where i is the iteration step and ϵ is the learning rate with a value greater than zero [21]. The learning stops when i reaches a given maximum number of iterations or when losses are lower than a certain small number [21].
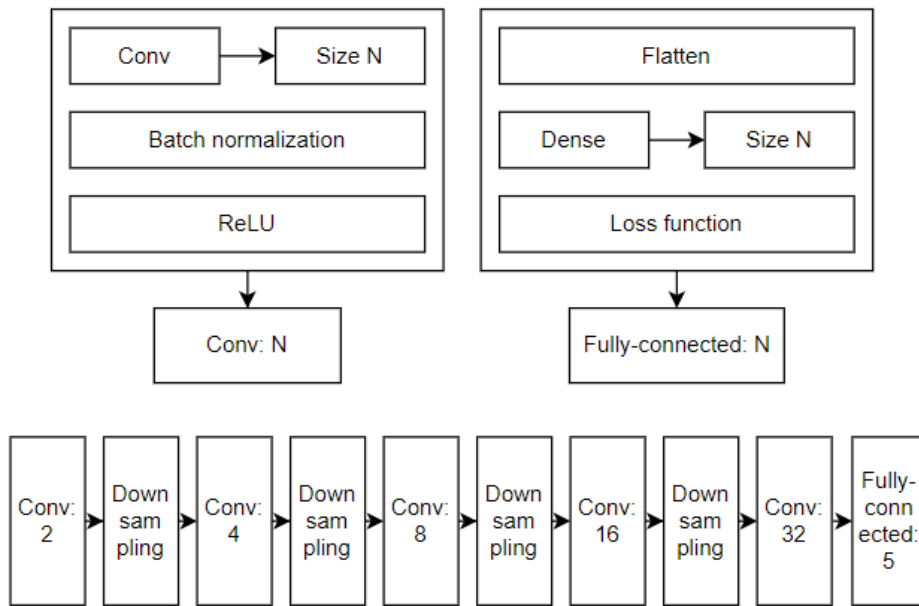
The resulting model can be represented as

Fig. 7. CNN model structure

This model represents complex functions, which correlates well with solving the problem of classifying the development stage of cardiomyocytes. At the same time, it is possible to observe the effect of degradation during deep learning (Fig. 8). The effect is expressed in a decrease of a validation accuracy (val_acuracy) that indicates the accuracy of classification of a randomly taken validation set after each training period compared to increase of the training accuracy (correct predictions over the training dataset).

This effect is due to the fact that deep networks often have a gradient signal that quickly goes to zero [23]. During the gradient descent, when returning from the last layer back to the first, multiplication by the weight matrix occurs at each step [23]. If the gradients are small due to the large number of multiplications, the gradient can decay to zero exponentially quickly.
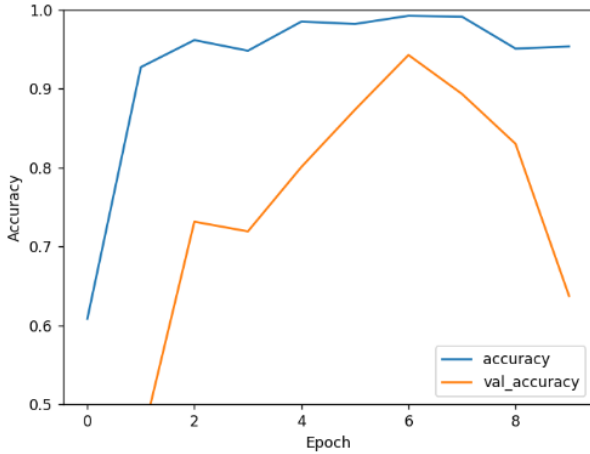
Fig. 8. CNN model degradation effect

The solution to this problem can be in using a residual block. The idea is that instead of learning the

layers on the base mapping, let the network match the residual mapping [23]. So, instead of the initial mapping $H(x)$, let the network fit $F(x)$:

$$F(x) = H(x) - x \Longrightarrow H(x) = F(x) + x. \qquad (9)$$

The approach is to omit the connection, which reduces the opportunity of the non-useful layer to affect the gradient signal [23]. Adding new layers will not harm the performance of the model, as the regularization will skip them if those layers are not useful. If the additional/new layers are useful, even with regularization, the weights or kernels of the layers will be non-zero and the model performance (classification accuracy) may increase (Fig. 9).

Such a model receives a processed image as an input and the result is a vector containing the probabilities that image belongs to each of the classes (development stage).
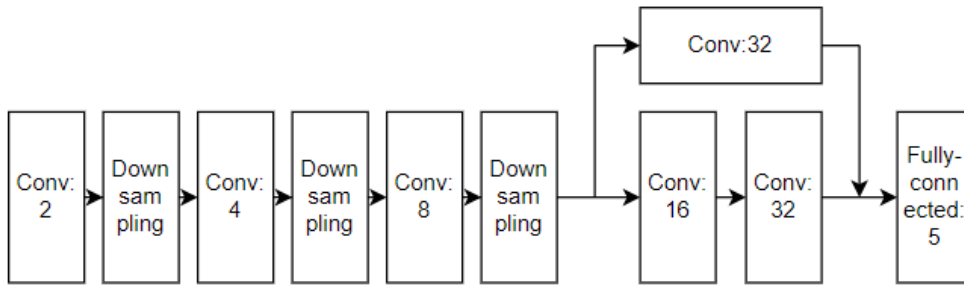

Fig. 9. CNN model structure with the residual block usage

3　CNN model training process

Data set is splitted into training and test data parts. The training set of 1036 images per each class (5180 images total) is additionally splitted with a split factor of 0.2, which corresponds to 80% of the training data (4144 images total for all classes) compared to the validation data (used to evaluate the model at each training step). The total accuracy estimate is calculated based on a total amount of true predictions across all classes and is performed after training on unused data (260 images per each class). Accuracy for each class separately is also calculated as the ratio of the amount of true predictions to the total number images in class. Results are presented in the form of a confusion matrix. Total accuracy is 62.62% (48.46% for class 1, 48.85% for class 2, 50% for class 3, 72.31% for class 4 and 93.46% for class 5). CNN model evolution and the training results can be seen in Fig. 10 and Fig. 11.

In Figure 11 each cell contains the amount of true or false predictions for each class comparatively to the total amount of testing images. True predictions are on the main diagonal and are included into the total accuracy estimate. Column "SUM" contains an

accuracy estimate per class (the ratio of the amount of true predictions to the total number of testing images in class).

The results can be analyzed using heat maps of different convolutional layers, which define the classification of the development stage of the cardiomyocytes (Fig. 12).
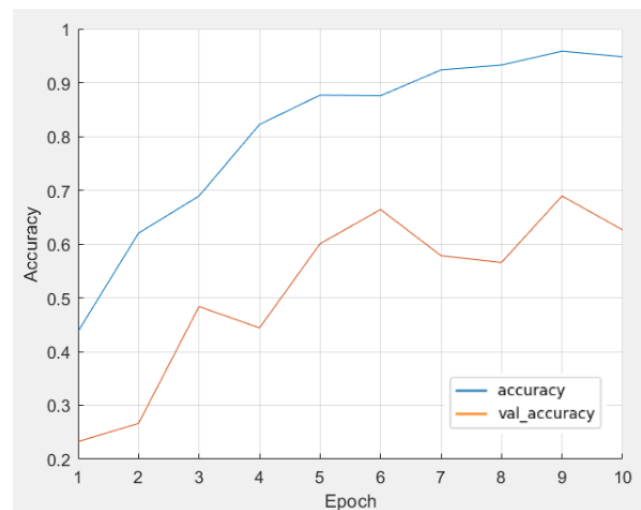

Fig. 10. CNN model evolution

Training Set						
TARGET OUTPUT	Class1	Class2	Class3	Class4	Class5	SUM
Class1	126 9.69%	54 4.15%	34 2.62%	28 2.15%	18 1.38%	260 48.46% 51.54%
Class2	23 1.77%	127 9.77%	52 4.00%	42 3.23%	16 1.23%	260 48.85% 51.15%
Class3	6 0.46%	15 1.15%	130 10.00%	87 6.69%	22 1.69%	260 50.00% 50.00%
Class4	11 0.85%	1 0.08%	23 1.77%	188 14.46%	37 2.85%	260 72.31% 27.69%
Class5	0 0.00%	0 0.00%	4 0.31%	13 1.00%	243 18.69%	260 93.46% 6.54%
SUM	166 75.90% 24.10%	197 64.47% 35.53%	243 53.50% 46.50%	358 52.51% 47.49%	336 72.32% 27.68%	814 / 1300 62.62% 37.38%

Fig. 11. Confusion matrix of the trained model
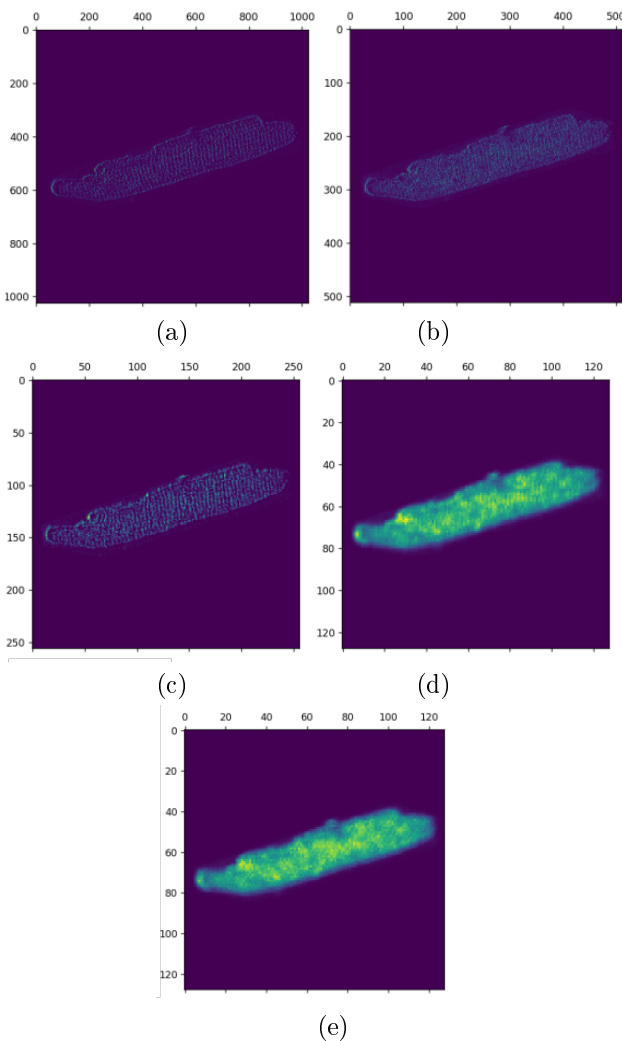

(a)

(b)

(c)

(d)

(e)

Fig. 12. Heat maps of convolutional layers: 2 (a), 4 (b), 8 (c), 16 (d), 32 (e)

It can be seen that the first layers of CNN highlight the shape and structure of cardiomyocytes, while the deeper layers increase the weights of factors that emphasize the structure of transverse T-tubules of a cardiomyocyte. It can also be shown by superimposing a heat map on the initial image of the cardiomyocyte. The reduction of the dimensionality of the heat map can be also seen, which is the result of the downsampling layer (Fig. 13).

(a)   (b)
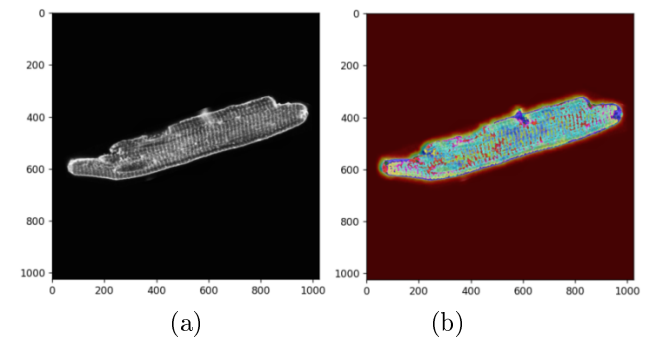
Fig. 13. Initial image (a) to the heat map (b) comparance

A large percentage of mutual errors between the first and second, as well as the third and fourth grades can be seen from the confusion matrix. This may indicate poor differentiation of the indicated development stages of cardiomyocytes.

The examples of images belonging to the first and second classes and classified with mutual errors are shown in Fig. 14. The weak differentiation of the

maturation stage of cardiomyocytes, as well as the focus of the heat map on the borders of cardiomyocytes but not on the structure of transverse T-tubules can be seen in heat-maps. This is due to their absence or early stage of their development. This also explains the high number of errors for the specified classes generally. A similar situation can be seen with images of the third and fourth classes (Fig. 15). Here, the structure of transverse T-tubules is poorly distinguished due to weak boundaries and a chaotic structure. Instead, a strong mutual differentiation of pairs of the first and second stages and the third and fourth stages can be seen.

(a)   (b)   (c)

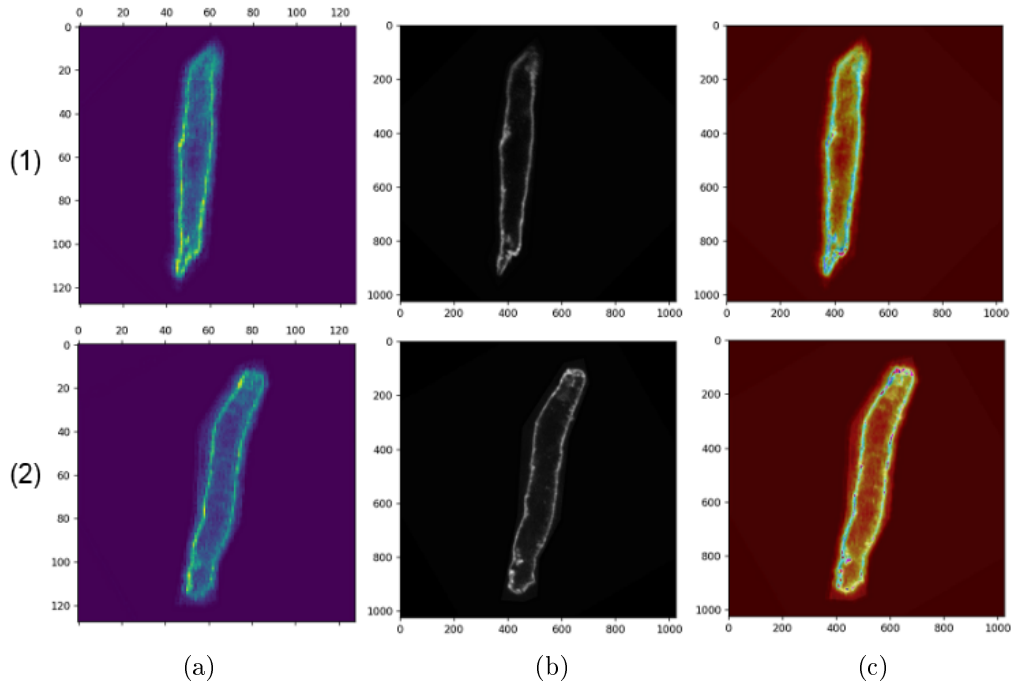Fig. 14. Heat map (a), initial image (b) and matching result (c) for the first (1) and second (2) classes

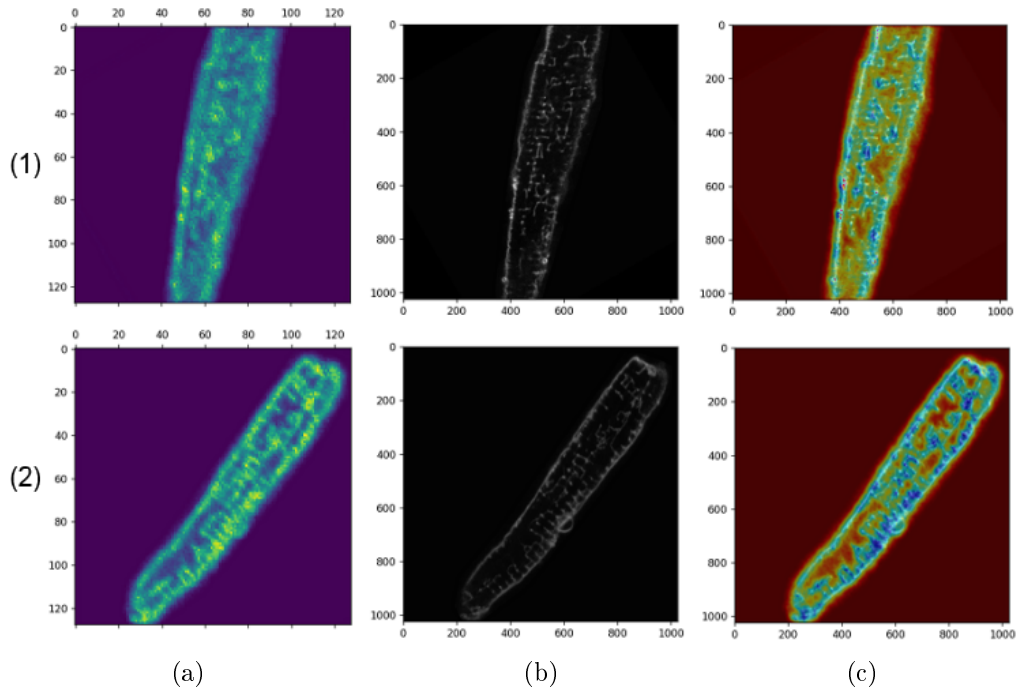(a)   (b)   (c)

Fig. 15. Heat map (a), initial image (b) and matching result (c) for the third (1) and fourth (2) classes

If we combine the classes that show a large number of mutual errors, namely, define the first and second classes as those that have an initial development stage, and the third and fourth – transitional, then after new model training and testing we have the following error matrix (Fig. 16).

Training Set				
TARGET / OUTPUT	Class1	Class2	Class3	SUM
Class1	330 25.38%	156 12.00%	34 2.62%	520 63.46% 36.54%
Class2	33 2.54%	428 32.92%	59 4.54%	520 82.31% 17.69%
Class3	0 0.00%	17 1.31%	243 18.69%	260 93.46% 6.54%
SUM	363 90.91% 9.09%	601 71.21% 28.79%	336 72.32% 27.68%	1001 / 1300 77.00% 23.00%

Fig. 16. Confusion matrix after class merging where class 1 is the initial development stage, class 2 is the transitional development stage and class 3 is developed cardiomyocytes

After combining the classes, the resulting accuracy reaches 77% (63.46% for initial development stage, 82.31% for the transitional development stage and 93.48% for developed cardiomyocytes). To further improve the classification accuracy, the architecture of CNN should be improved using deeper layers and more original cardiomyocyte images should be extracted.

It should be noted that increasing the amount of data by augmentation does not provide the proper improvement in classification accuracy.

For comparison, the first approach to preparing the training data set (to choose the number of images in each class according to the minimum amount with the use of the unused data to evaluate the trained model) with a dramatical increasing percentage of augmented data was used. Here, training took place in several iterations due to the large amount of data. The resulting accuracy of this approach is 64% without combining classes. The increase in the training accuracy estimate is due to the fact that the validation data may contain features or parts of the training images that affect the training accuracy estimate (Fig. 17).

Conclusion

Research methods of the cardiomyocytes grown from the pluripotent stem cells and the main directions of their use were considered. Also, the need for automated recognition of their maturation stage was shown.
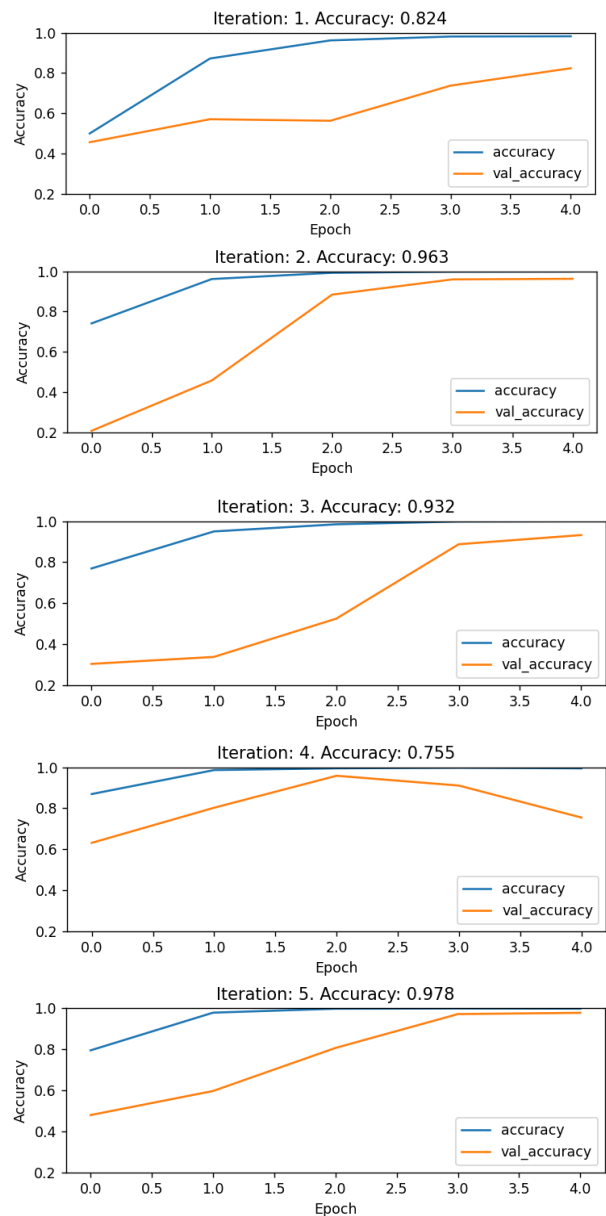

Fig. 17. CNN model training with high augmented images percentage

The original data set (pre-classified confocal images of cardiomyocytes) is prepared by digital image processing methods, which includes segmentation, brightness histogram processing and augmentation. The Chan–Vese method, which belongs to the regional segmentation methods, is chosen as the segmentation method. It does not depend on the image gradient and can segment objects with weak boundaries and is robust to noise due to the use of global region information. To process the image brightness histogram, the method of contrast-limited adaptive equalization is used, which has the ability to improve the local contrast of the image and reduce noise in the resulting image. For augmentation, methods (image rotation and flipping) that prevent the alteration of the transverse T-tubule, which is an important parameter for correct classification, and also do not affect the

contrast of the image, which is an important parameter for highlighting the structure of the transverse T-tubule were used. To perform the equalization of the number of images in each class, the color inversion method is used, which also does not affect the structure of the transverse T-tubule and does not greatly affect the differentiation of the augmented data. The resulting amount of images after augmentation is 1296 for each stage of cardiomyocyte maturation, 1036 of them are used as training data.

To solve the problem of classification of the development stage of cardiomyocytes, a convolutional neural network is used, which has high performance when working with images. The architecture of a convolutional neural network with a hierarchical structure and residual block usage is built and trained based on the prepared data.

The evolution of model training and heat maps of different convolutional layers are shown. The classification accuracy is evaluated using images not used in training. The resulting accuracy is 62.62% for 5 classes classification task (48.46% for class 1, 48.85% for class 2, 50% for class 3, 72.31% for class 4 and 93.46% for class 5). The confusion matrix and images of classes that showed a large number of mutual errors were analyzed. Based on the analysis, the classes were combined. The images of the first and second classes are assigned to the initial stage of development, and the third and fourth – to the transitional stage. After merging, the accuracy of the model for 3 maturation stages recognition achieved 77% (63.46% for initial development stage, 82.31% for the transitional development stage and 93.48% for developed cardiomyocytes).

Based on the results of the analysis, it was pointed out the need for further research in the field of growing cardiomyocytes from pluripotent stem cells in order to highlight more original images of cardiomyocytes and determine more accurate classification parameters. Further increasing the number of images using augmentation methods and the number of iterations during training does not give the desired results.

References

[1] Lainscak, M., Spoletini, I., & Coats, A. J. (2017). Definition and Classification of Heart Failure. *International Cardiovascular Forum Journal*, Vol. 10, pp. 3-7, DOI: 10.17987/icfj.v10i0.419.

[2] The top 10 causes of death. *World Health Organization*, date of access: 7 August 2024.

[3] Savarese G., Becher P. M., Lund L. H., Seferovic P., Rosano G. M. C., Coats A. J. S. (2022). Global burden of heart failure: a comprehensive and updated review of epidemiology. *Cardiovascular Research*, Vol. 118, Iss. 17, pp. 3272–3287, doi:10.1093/cvr/cvac013.

[4] Donald M. Bers (2001). *Excitation-Contraction Coupling and Cardiac Contractile Force (2nd ed.).* Kluwer Academic Publishers, 427 p., doi:10.1007/978-94-010-0658-3.

[5] Reinecke H., Minami E., Zhu W. Z., Laflamme M. A. (2008). Cardiogenic Differentiation and Transdifferentiation of Progenitor Cells. *Circulation Research*, Vol. 103, Num. 10, pp. 1058–1071, doi:10.1161/CIRCRESAHA.108.180588.

[6] Zhu W. Z., Hauch K. D., Xu C., Laflamme M. A. (2009). Human embryonic stem cells and cardiac repair. *Transplant Rev (Orlando)*, Vol. 23, Iss. 1, pp. 53-68, doi:10.1016/j.trre.2008.05.005.

[7] Kupatt C., Horstkotte J., Vlastos G. A., Pfosser A., Lebherz C., Semisch M., et al. (2005). Embryonic endothelial progenitor cells expressing a broad range of pro-angiogenic and remodeling factors enhance vascularization and tissue recovery in acute and chronic ischemia. *The FASEB Journal*, Vol. 19, Iss. 11, doi:10.1096/fj.04-3282fje.

[8] Caspi O., Huber I., Kehat I., Habib M., Arbel G., Gepstein A., et al. (2007). Transplantation of Human Embryonic Stem Cell-Derived Cardiomyocytes Improves Myocardial Performance in Infarcted Rat Hearts. *Journal of the American College of Cardiology*, Vol. 50, Iss. 19, pp. 1884-1893, doi:10.1016/j.jacc.2007.07.054.

[9] Shimizu T., Yamato M., Kikuchi A., Okano T. (2003). Cell sheet engineering for myocardial tissue reconstruction. *Biomaterials*, Vol. 24, Iss. 13, pp. 2309-2316, doi:10.1016/S0142-9612(03)00110-8.

[10] Pointon A., Harmer A. R., Dale I. L., Abi-Gerges N., Bowes J., Pollard C., Garside H. (2015). Assessment of Cardiomyocyte Contraction in Human-Induced Pluripotent Stem Cell-Derived Cardiomyocytes. *Toxicological Sciences*, Vol. 144, Iss. 2, pp. 227–237, doi:10.1093/toxsci/kfu312.

[11] Zhu, W.-Z., Van Biber, B., and Laflamme, M. A. (2011). Methods for the Derivation and Use of Cardiomyocytes from Human Pluripotent Stem Cells. In: Schwartz, P., Wesselschmidt, R. (eds) Human Pluripotent Stem Cells. *Methods in Molecular Biology*, Vol. 767, pp. 419–431, doi:10.1007/978-1-61779-201-4_31.

[12] Zahradnikova jr. A., Skrabanek P. (2019). Confocal microscopy images of cardiomyocyte development stages. *IEEE DataPort*, date of access: sept. 2023.

[13] Shigang Liu, Yali Peng. (2012). A local region-based Chan–Vese model for image segmentation. *Pattern Recognition*, Vol. 45, Iss. 7, pp. 2769-2779, doi:10.1016/j.patcog.2011.11.019.

[14] Getreuer P. (2012). Chan-Vese Segmentation. *Image Processing On Line*, Vol. 2, pp. 214–224, doi:10.5201/ipol.2012.g-cv.

[15] Pizer S. M., Johnston R. E., Ericksen J. P., Yankaskas B. C. and Muller K. E. (1990). Contrast-limited adaptive histogram equalization: speed and effectiveness. *Proceedings of the First Conference on Visualization in Biomedical Computing*, pp. 337-345, doi:10.1109/VBC.1990.109340.

[16] Vij K., Singh Y. (2009). Enhancement of Images Using Histogram Processing Techniques. *Int. J. Comp. Tech. Appl.*, Vol. 2, Iss. 2, pp. 309-313.

[17] Shorten, C., Khoshgoftaar, T. M. (2019). A survey on Image Data Augmentation for Deep Learning. *Journal of Big Data*, Vol. 6, Article number: 60, doi:10.1186/s40537-019-0197-0.

[18] Gaster B. R., Howes L., Kaeli D. R., Mistry P., Schaa D. (2013). *Heterogeneous Computing with OpenCL*. Morgan Kaufmann Publishers Inc., 291 p.

[19] Grossi E., Buscema M. (2007). Introduction to artificial neural networks. *European Journal of Gastroenterology & Hepatology*, Vol. 19, Iss. 12, pp. 1046-1054, DOI: 10.1097/MEG.0b013e3282f198a0.

[20] Purwono, P., Ma'arif, A., Rahmaniar, W., Fathurrahman, H., Frisky, A., & Haq, Q. (2022). Understanding of Convolutional Neural Network (CNN): A Review. *International Journal of Robotics and Control Systems*, Vol. 2, No. 4, pp. 739-748, doi:10.31763/ijrcs.v2i4.888.

[21] Alpaydin, E. (2010). *Introduction to Machine Learning*, Second Edition. The MIT Press, 579 p., ISBN 978-0-262-01243-0.

[22] Ziaee A. and ÇAno E. (2022). Batch Layer Normalization A new normalization layer for CNNs and RNNs. *ICAAI'22: Proceedings of the 2022 6th International Conference on Advances in Artificial Intelligence*, pp. 40-49, doi:org/10.1145/3571560.3571566.

[23] Ebrahimi, M. S., & Abadi, H. K. (2018). Study of Residual Networks for Image Recognition. *ArXiv*, doi:10.48550/arXiv.1805.00325.

Класифікація стадії структурно-функціонального розвитку кардіоміоцитів за допомогою методів машинного навчання

Бондарєв В. Р., Іванько К. О., Іванушкіна Н. Г.

Дослідження присвячено проблемі класифікації стадії структурно-функціонального дозрівання кардіоміоцитів, отриманих з індукованих плюрипотентних стовбурових клітин, із застосуванням методів цифрової обробки зображень та алгоритмів машинного навчання, зокрема нейронних мереж. Клітинна регенеративна терапія стала одним із найбільш перспективних варіантів лікування пацієнтів із серцевою недостатністю. Але оскільки кардіоміоцити є об'єктами високого рівня складності та мають значну морфологічну мінливість, автоматична класифікація ускладнюється відсутністю реалізованих методів. Тому дослідження в цій галузі є важливим пріоритетом в галузі охорони здоров'я. Початковий набір даних, використаний у цьому дослідженні, є загальнодоступним набором конфокальних мікроскопічних зображень кардіоміоцитів, які можна розділити на п'ять класів на основі морфологічних ознак (структури поперечних Т-канальців). Невеликий обсяг вхідних даних призводить до необхідності використання методів аугментації. Використовувалися методи, що запобігають альтерації поперечного Т-канальця, що є важливим параметром для правильної класифікації стадії розвитку кардіоміоцитів. Для підвищення контрастності та динамічного діапазону конфокальних мікроскопічних зображень використовувався метод вирівнювання гістограми за допомогою методу адаптивного вирівнювання з обмеженим контрастом. Це дозволило покращити локальний контраст зображень і виділити основні структурні елементи кардіоміоцитів. Нарешті, метод Чан-Везе, який належить до методів регіональної сегментації, був обраний для сегментації зображень та видалення артефактів та/або частин інших клітин із зображень. Оброблений і аугментований набір даних використовувався для навчання згорткової нейронної мережі, що має архітектуру з ієрархічною структурою та використанням залишкових блоків. Модель було оцінено на основі матриці помилок, також було проаналізовано теплові карти різних згорткових шарів. Були розглянуті зображення з класів з великою кількістю взаємних помилок. На основі проведеного аналізу декілька класів структурно-функціонального розвитку кардіоміоцитів були об'єднані. Остаточна точність моделі для визначення стадії дозрівання кардіоміоцитів досягла 77%.

Ключові слова: кардіоміоцит; стовбурові клітини; обробка зображень; машинне навчання; проблема машинного навчання; класифікація; точність класифікації; нейронна мережа; згорткова нейронна мережа